

Photon mediated energy, linear and angular momentum transport in fullerene and graphene systems beyond local equilibrium

Jian-Sheng Wang^{1,2} and Mauro Antezza^{2,3}

¹*Department of Physics, National University of Singapore, Singapore 117551, Republic of Singapore*

²*Laboratoire Charles Coulomb (L2C), UMR 5221 CNRS-Université de Montpellier, F-34095 Montpellier, France*

³*Institut Universitaire de France, 1 rue Descartes, F-75231 Paris, France*

(Dated: 21 July 2023, revised again 23 February 2024)

Based on a tight-binding model for the electron system, we investigate the transfer of energy, momentum, and angular momentum mediated by electromagnetic fields among buckminsterfullerene (C_{60}) and graphene nano-strips. Our nonequilibrium Green's function approach enables calculations away from local thermal equilibrium where the fluctuation-dissipation theorem breaks down. For example, the forces between C_{60} and current-carrying nano-strips are predicted. It is found that the presence of current enhances the van der Waals attractive forces. For two current-carrying graphene strips rotated at some angle, the fluctuational force and torque are much stronger at the nanoscale compared to that of the static Biot-Savart law.

Keywords: quantum transport, thermal radiation, Casimir force, nonequilibrium Green's function.

I. INTRODUCTION

Energy transfer can be carried out in three forms – conduction, convection, and radiation [1]. Radiation is special in that we do not need a material medium for the transfer. Energy can be transmitted in a vacuum. From the past half a century of work, it has been established that energy transfers are enhanced when objects are in the near field [2–4]. This has been verified by many experiments [5–10] and theoretical calculations [11–15]. Such near-field effects have also found many applications [16].

A related transport phenomenon is the transfer of momentum. This is the origin of the van der Waals or London attractive forces [17] at short distances and Casimir [18–21] or Casimir-Polder forces [22, 23] at a larger distance when the finite speed of light is taken into account. An atom above a dielectric surface is a classic problem that has been investigated extensively [22, 24, 25]. Progress has been made on subtle effects of the temperatures of the bodies [26–30].

So far, even for the global nonequilibrium situations, most of the theoretical developments have been based on the assumption of local thermal equilibrium [4, 19], where each object still satisfies the fluctuation-dissipation theorem. Systems driven by the electric current can be modeled by a Doppler shift of the equilibrium conductivities phenomenologically [31–34]. The effect of the temperature gradient of the objects has only been investigated recently [35–37]. These investigations couple the heat radiation with the diffusion equation or Boltzmann transport theory, still at a macroscopic or mesoscopic level. Another approach to nonequilibrium transport is to modify the Bose function with chemical potential bias [38]. Our motivation here is to work at the microscopic level, starting with a model of matter as electrons hopping on some (lattice) sites. Thus, the nonequilibrium

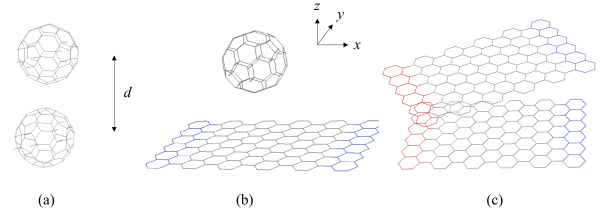


FIG. 1. Schematic configurations of carbon systems. (a) The configuration of a C_{60} molecule with a center-to-center distance $d = 1$ nm away from another C_{60} . (b) C_{60} above a 13×8 armchair graphene strip. The strip is approximately a square of length 1.5 nm. The C_{60} is positioned at the center of the square. (c) Two strips rotated by 30° . Only parts of the bath sites and bonds in color are shown explicitly.

aspect can be handled from first principles, using the Keldysh nonequilibrium Green's function (NEGF) formalism [39–42]. The drawback, of course, is computational complexity, which limits the method to small systems at the nanoscale. Along this line, a general photon transport theory for energy, momentum, and angular momentum has been developed under the framework of the nonequilibrium Green's function formulation [43–45]. It reduces to the usual fluctuational electrodynamics [46–48] if a local thermal equilibrium is valid. The objects can be put out of local thermal equilibrium by connecting to two or more baths at different temperatures or chemical potentials, causing the objects to have heat or electric current. An out-of-equilibrium system breaks reciprocity even though the Hamiltonian is still reciprocal in the sense $H^T = H$; here, H is the single particle Hamiltonian matrix, and the superscript T denotes matrix transpose.

In this paper, we demonstrate the power of the NEGF formalism for fullerene systems consisting of the C_{60} molecules and graphene strips in the armchair geome-

try. Specifically, we consider the transfer of conserved quantities between C_{60} and C_{60} molecules, C_{60} with a flat graphene strip, and between two strips rotated at an angle (see Fig. 1).

In the following, we give a recipe for calculation. The derivations of these formulas are already presented in Refs. [43–45], except for more computational details. We define the model considered, present the numerical results, and discuss their significance. In the Appendices, we give a quick derivation of the Meir-Wingreen formula and relate it to the Casimir-Polder formula for van der Waals forces.

II. MODEL

We consider systems as objects described by a tight-binding model of the form $\sum_{jk} c_j^\dagger H_{jk}^\alpha c_k$ of spinless free electrons. Each object α is connected to a number of baths or electron reservoirs so that the number of electrons on the objects can fluctuate, and the reservoirs define their thermal properties. The baths can also have chemical potential bias so that the object may have an electric current. All this is described by additional electron self-energies Σ due to the baths so that the electron Green's functions for the object α are [49]

$$G_\alpha^r(E) = \left(E + i\eta - H^\alpha - \sum \Sigma^r(E) \right)^{-1}, \quad (1)$$

$$G_\alpha^{<,>}(E) = G_\alpha^r(E) \sum \Sigma^{<,>}(E) G_\alpha^a(E), \quad (2)$$

where the first line is the retarded Green's function, and the second line is the lesser (<) and greater (>) Green's functions which are given by the Keldysh equations. The advanced Green's function is obtained by the Hermitian conjugate of the retarded one, $G^a = (G^r)^\dagger$, and the sum indicates the possibility of many baths for each object. We assume that each bath is in thermal equilibrium so that we have the fluctuation-dissipation theorems for $\Sigma^{<,>}$. That is, $\Sigma^{<} = -f(\Sigma^r - \Sigma^a)$, $\Sigma^{>} = (1-f)(\Sigma^r - \Sigma^a)$, where $f = 1/(\exp((E-\mu)/(k_B T)) + 1)$ is the Fermi function. Thus, each bath is characterized by two parameters: the temperature T and the chemical potential μ . In particular, to be consistent, the damping of the center, η , is also counted as one of the baths. This central bath can be interpreted as the substrate or gate applied to the system.

The electron-field interaction is described in the scalar potential $\phi = 0$ gauge with the Peierls substitution Hamiltonian [50], $\sum_{jk} c_j^\dagger H_{jk} c_k \exp\left(-i\frac{e}{\hbar} \int_{\mathbf{R}_k}^{\mathbf{R}_j} \mathbf{A} \cdot d\mathbf{r}\right)$. Here c_j^\dagger is the creation operator of the electron at site j , c_k is the annihilation operator at site k , and \mathbf{A} is the vector potential. The electron-photon interaction matrices can be obtained from the Hamiltonian and the locations of the sites, via the velocity matrix:

$$\mathbf{V}_{jk}^\alpha = \frac{1}{i\hbar} H_{jk}^\alpha (\mathbf{R}_j - \mathbf{R}_k), \quad (3)$$

where \mathbf{R}_j is the three-dimensional vector of the location of site j . We introduce an \mathbf{M}^l matrix so that a sum over site l produces $e\mathbf{V}^\alpha$, by

$$M_{jk}^{l\mu} = \frac{1}{2} e (\delta_{lj} + \delta_{lk}) V_{jk}^{\alpha,\mu}, \quad \mu = x, y, z, \quad (4)$$

i.e., \mathbf{M}^l is half of the l -th row and l -th column of the \mathbf{V}^α matrix times e , here e (> 0) is the magnitude of the elementary charge.

III. PHOTON SELF-ENERGIES AND MEIR-WINGREEN FORMULAS

In the usual approach to fluctuational electrodynamics [51, 52], the material property for electromagnetic response is given by a frequency-dependent local dielectric function. Such a description would not be suitable when the system is at the nanoscale, such as a C_{60} molecule. In the NEGF approach, the dielectric function is replaced by nonlocal quantities (matrices in site l and direction μ) that we call self-energies. These are the self-energies for the photon interacting with the electrons. It is a key step in the calculation. Under the random-phase approximation, they are given by the current-current correlations [45],

$$\begin{aligned} \Pi_{l\mu,\nu}^{<}(\omega) = & \\ & -2i \int_{-\infty}^{+\infty} \frac{dE}{2\pi} \text{Tr} [M^{l\mu} G^{<}(E) M^{l\nu} G^{>}(E - \hbar\omega)], \end{aligned} \quad (5)$$

$$\begin{aligned} \Pi_{l\mu,\nu}^r(\omega) = & \\ & -2i \int_{-\infty}^{+\infty} \frac{dE}{2\pi} \text{Tr} \left[M^{l\mu} G^r(E + \hbar\omega) M^{l\nu} G^{<}(E) + \right. \\ & \left. M^{l\mu} G^{<}(E) M^{l\nu} G^a(E - \hbar\omega) \right]. \end{aligned} \quad (6)$$

The greater version $\Pi^{>}$ is obtained by swapping lesser with greater for the electron Green's functions. The Keldysh version is defined as $\Pi^K = \Pi^{<} + \Pi^{>}$, and advanced version is $\Pi^a = (\Pi^r)^\dagger$. Here, the dagger means taking complex conjugate and transposing in both the space and the direction index, (l, μ) . The extra factor of 2 is for the spin degeneracy. The retarded self-energy is related to the conductivity in a continuum description by $\sigma = i\Pi^r/\omega$ [53].

The self-energies, also known as polarizabilities, are the critical inputs for the transport calculations. The numerical accuracy of the energy integration needs to be maintained to high standards. The broadening parameter η controls the integration spacings. We choose this spacing a few times smaller than η , and look for convergence.

A. Diamagnetic term

The diamagnetic term is needed to correctly describe the plasmon physics of the electrons. For the retarded

Π^r , this term has no imaginary part; thus, it is nondissipative, describing the motion of the electrons in response to the external field.

If we expand the Peierls substitution term to second order in the vector field, using the trapezoidal rule for the line integral, the extra interaction responsible for the diamagnetic term is

$$H' = -\frac{e^2}{8\hbar^2} \sum_{jk\mu\nu} c_j^\dagger H_{jk} c_k (A_j^\mu + A_k^\mu) (R_j^\mu - R_k^\mu) \times (A_j^\nu + A_k^\nu) (R_j^\nu - R_k^\nu). \quad (7)$$

The contribution to the Dyson expansion of the contour ordered Green's function $D_{\alpha\beta}(\mathbf{r}, \tau; \mathbf{r}', \tau')$ = $\langle T_\tau A_\alpha(\mathbf{r}, \tau) A_\beta(\mathbf{r}', \tau') \rangle / (i\hbar)$ due to this interaction is (at the lowest order)

$$\begin{aligned} & \left(\frac{1}{i\hbar} \right)^2 \left\langle T_\tau A_\alpha(\mathbf{r}, \tau) \int d\tau'' H'(\tau'') A_\beta(\mathbf{r}', \tau') \right\rangle \\ &= \frac{e^2}{8\hbar^4} \sum_{jk\mu\nu} \int d\tau'' \left\langle T_\tau A_\alpha(\mathbf{r}, \tau) \left[A_j^\mu(\tau'') A_j^\nu(\tau'') + \right. \right. \\ & \quad \left. \left. A_k^\mu(\tau'') A_k^\nu(\tau'') + A_j^\mu(\tau'') A_j^\nu(\tau'') + A_k^\mu(\tau'') A_k^\nu(\tau'') \right] \times \right. \\ & \quad \left. A_\beta(\mathbf{r}', \tau') \right\rangle H_{jk} \langle c_j^\dagger(\tau'') c_k(\tau'') \rangle \times \\ & \quad (R_j^\mu - R_k^\mu) (R_j^\nu - R_k^\nu). \end{aligned} \quad (8)$$

Here τ, τ', τ'' are Keldysh contour times, and T_τ is the contour order super-operator. To the lowest order, we can separate the averages in photon space from that of electron space. The next step is to apply Wick's theorem for the \mathbf{A} field and express the field correlation by the photon Green's function. To identify the self-energy, we write the final expression in the form $D\Pi D$, as a convolution in contour times and space (as discrete sums). The extra diamagnetic self-energy is

$$\begin{aligned} \Pi_{\mu, \nu}^{\text{dia}}(\tau_1, \tau_2) &= \frac{ie^2}{2\hbar} \delta(\tau_1, \tau_2) \sum_{jk} \left[\delta_{lj} \delta_{l\nu j} + \delta_{lj} \delta_{l\nu k} + \right. \\ & \quad \left. \delta_{lk} \delta_{l\nu j} + \delta_{lk} \delta_{l\nu k} \right] (R_j^\mu - R_k^\mu) (R_j^\nu - R_k^\nu) H_{jk} G_{kj}^<(0). \end{aligned} \quad (9)$$

Here $G^<(t)$ is the lesser Green's function of the electron in the time domain. A factor of 2 has been multiplied for the spin degeneracy. The final result is proportional to a delta function in contour time. This means that there is no contribution to $\Pi^<$ and $\Pi^>$. We only pick up a retarded component, $\Pi^r = \Pi^t - \Pi^<$, which is a constant in the frequency domain, due to the delta function $\delta(t_1 - t_2)$ in the time domain. Here Π^t is the time-ordered version of the self-energy. On a continuum, this diamagnetic term is $-e^2 n/m$; here, n is electron density. It is also equal to the negative of current-current correlation at zero frequency, $-\Pi^r(\omega = 0)$, from gauge invariance. On a lattice, it is somewhat more complicated due to our use of Peierls substitution Hamiltonian.

B. Free-field photon Green's function

The photon Green's function $D = -\mu_0 G$ is the same as the usual dyadic Green's function G up to a numerical factor of $-\mu_0$, which is the vacuum permeability. In a vacuum without matter, we use the symbol v to denote the free photon Green's function, which is given explicitly by the formula [54, 55]

$$v^r(\mathbf{r}, \omega) = -\frac{e^{i\frac{\omega}{c}r}}{4\pi\epsilon_0 c^2 r} \left\{ (\overset{\leftrightarrow}{\mathbf{U}} - \hat{\mathbf{R}}\hat{\mathbf{R}}) + \left[-\frac{1}{i\frac{\omega}{c}r} + \frac{1}{(i\frac{\omega}{c}r)^2} \right] (\overset{\leftrightarrow}{\mathbf{U}} - 3\hat{\mathbf{R}}\hat{\mathbf{R}}) \right\}. \quad (10)$$

Here $\overset{\leftrightarrow}{\mathbf{U}}$ is the identity dyadic, $\hat{\mathbf{R}} = \mathbf{r}/r$ is the radial direction unit vector.

To compute the force and torque, we also need the derivative of this expression with respect to space. We obtain in component form a messy formula as

$$\begin{aligned} \partial_\mu v_{\alpha\beta}^r &= \frac{e^X}{4\pi\epsilon_0 c^2 r^2} \left[\left(2 - X - \frac{3}{X} + \frac{3}{X^2} \right) \hat{R}_\mu \delta_{\alpha\beta} + \right. \\ & \quad \left(-6 + X + \frac{15}{X} - \frac{15}{X^2} \right) \hat{R}_\mu \hat{R}_\alpha \hat{R}_\beta + \\ & \quad \left. \left(1 - \frac{3}{X} + \frac{3}{X^2} \right) (\delta_{\mu\alpha} \hat{R}_\beta + \delta_{\mu\beta} \hat{R}_\alpha) \right], \end{aligned} \quad (11)$$

where $X = i\omega r/c$, and μ, α , or β takes the x, y , or z direction. \hat{R}_μ is the component of the unit vector $\hat{\mathbf{R}}$ in the μ direction.

In computing the transported quantities with the Meir-Wingreen formulas, we only need the values of D at the electron sites. Hence, the free Green's function is also evaluated at a discrete set of distances $\mathbf{r} = \mathbf{R}_j - \mathbf{R}_k$, where \mathbf{R}_j and \mathbf{R}_k are the tight-binding sites. The Dyson equation $D^r = v^r + v^r \Pi^r D^r$ is a $3N \times 3N$ matrix equation for N electron sites. The extra factor of 3 is due to the x, y , and z directions for each site. The two formulas, Eq. (10) and (11), diverge at $\mathbf{r} = 0$, and thus cannot be used. The divergence is due to our approximation of electrons to be point-like. In reality, the wave functions of the electrons are extended with sizes of order angstrom. To deal with this divergence, we need a cut-off distance $r_c = 2$ Hartree atomic units (a.u.). When $r < r_c$, we reset r to be r_c with $\hat{\mathbf{R}} = 0$. This gives, following Refs. [56, 57], $v^r(\mathbf{0}, \omega) \approx \frac{1}{4\pi\epsilon_0 \omega^2 r_c^3} \overset{\leftrightarrow}{\mathbf{U}}$, and $\nabla v^r = 0$. The results are sensitive to the value r_c as it reflects the screening in the dielectric matrix $\epsilon = 1 - v^r \Pi^r$. The value r_c is determined from the Coulomb energy of two overlapping p -orbitals. With the choice of $r_c = 2$ a.u., it gives a reasonable screening strength for carbon atoms with a static dielectric constant close to 3 (as compared by the screened and bare polarizability α of C_{60}).

C. Dyson equation and Meir-Wingreen formulas

With these preparations, we solve the Dyson equation,

$$D^r = v^r + v^r \sum_{\alpha} \Pi_{\alpha}^r D^r, \quad (12)$$

and calculate the derivatives by $\nabla D^r = \nabla v^r + \nabla v^r \sum_{\alpha} \Pi_{\alpha}^r D^r$.

We also need the Keldysh version for distribution, which is obtained by $D^K = D^r \sum_{\alpha} \Pi_{\alpha}^K D^a$, and the advanced version by $D^a = (D^r)^{\dagger}$. In calculating the Keldysh equation, we have ignored one term, the bath at infinity, Π_{∞}^K . This term represents the dissipation of energy to infinity. When several objects are close, the magnitudes of their energy transfer are much larger than those transferred to infinity, so omitting it is justifiable. We can have another formula for these emitted to infinity by integrating the Poynting vector or Maxwell's stress tensor on a sphere. We note that conservation laws break down in our approximation here.

Finally, the Meir-Wingreen formulas for the energy transferred out from object α , force and torque applied to object α , are [45],

$$\frac{d\langle \hat{O} \rangle}{dt} = \text{Re} \int_0^{\infty} \frac{d\omega}{2\pi} \text{Tr} \left[\hat{O} (D^r \Pi_{\alpha}^K + D^K \Pi_{\alpha}^a) \right], \quad (13)$$

where \hat{O} is the operator $-\hbar\omega$ for energy transfer, $-i\hbar\nabla$ for force, and $\mathbf{r} \times (-i\hbar\nabla) + \mathbf{S}$ for torque [58]. Here $S_{\mu\nu}^{\gamma} = (-i\hbar)\epsilon_{\mu\nu\gamma}$ is the spin angular momentum operator expressed in the Levi-Civita symbol. These operators act on the first argument of space and direction of the photon Green's function D . The trace is a sum of the discrete site indices and the directions.

We comment that if the system has an overall thermal equilibrium in the sense $\Pi^K = (2N + 1)(\Pi^r - \Pi^a)$ and similarly for D^K , we can transform the factor $D^r \Pi_{\alpha}^K + D^K \Pi_{\alpha}^a$ to $2i(2N + 1)\text{Im}(D^r \Pi_{\alpha}^r)$ (for reciprocal systems). Here $N = 1/(\exp(\hbar\omega/(k_B T)) - 1)$ is the Bose function. This will give 0 energy currents, but the force and torque are not zero. We can further transform $\text{Im}(D^r \Pi_{\alpha}^r)$ into the Matsubara frequencies, $\omega \rightarrow i\omega_n$, making a contact with the Lifshitz theory for Casimir force [19, 24, 59, 60]. The formulas should be numerically more stable in the imaginary frequencies as the functions are not oscillatory. However, the drawback is that we can no longer handle nonequilibrium problems. The Matsubara sum form for the equilibrium system is then

$$\frac{d\langle \hat{O} \rangle}{dt} = \frac{2k_B T}{\hbar} \sum_{n \geq 0} \text{Tr} \left[(i\hat{O}) D^r(i\omega_n) \Pi_{\alpha}^r(i\omega_n) \right], \quad (14)$$

where the prime means that the $n = 0$ term has a weight of 1/2. The Matsubara frequencies take the values $\omega_n = 2\pi n k_B T / \hbar$.

Since the derivative of v^r is antisymmetric, any symmetric matrix multiplying it and taking trace is 0.

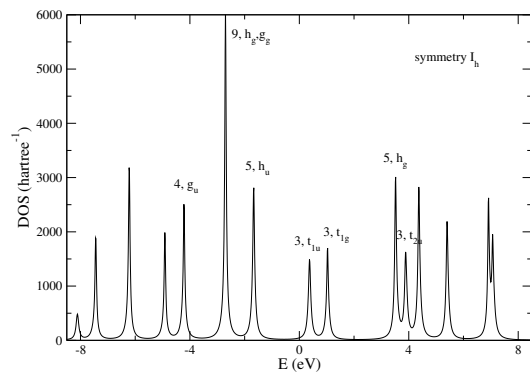


FIG. 2. The density of states of C₆₀. Some of the peaks are marked by the degeneracy and the orbital symmetry labels.

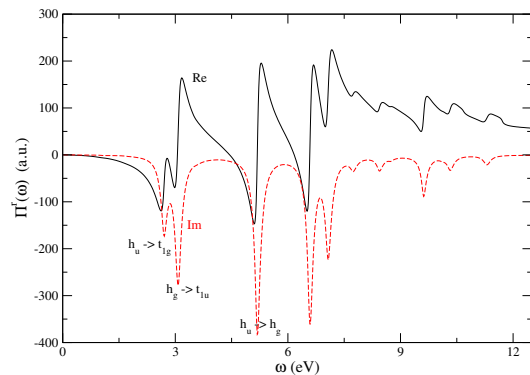


FIG. 3. Sum total of the retarded photon self-energy $\Pi^r(\omega)$ in atomic units. The solid line is for the real part, and the dashed line is for the imaginary part. Some of the peaks are marked with corresponding electron state transitions.

Using this property, for reciprocal systems, we can omit the $\nabla v^r \Pi_{\alpha}^r + \nabla v^r \Pi_{\alpha}^r D^r \Pi_{\alpha}^r$ terms, and use only $\nabla v^r \sum_{\beta \neq \alpha} \Pi_{\beta}^r D^r \Pi_{\alpha}^r$ [61]. The omitted terms, which constitute the self-interaction force, are zero for equilibrium systems. This improves numerical stability for the force calculation.

IV. C₆₀-C₆₀ VAN DER WAALS FORCE

We use the coordinates for C₆₀ of Ref. [62], assuming a nearest neighbor hopping of $t = 2.7$ eV [63]. The molecule is rotated 90° along the x direction so that the z axis becomes y in our coordinate system, see Fig. 1.

The density of states (DOS) and the calculated Π^r are presented in Fig. 2 and 3. The C₆₀ molecule has the symmetry group I_h ; thus, the states are highly degenerate. Some states near the Fermi energy $\mu = 0$ eV are labeled by their degeneracy and orbital symmetry. The lowest occupied and highest unoccupied states have a gap of 2.04 eV. The DOS is calculated according to $-\text{Im} \text{Tr} G^r(E)$. A damping of $\eta = 27$ meV in the electron Green's function is used throughout all the cal-

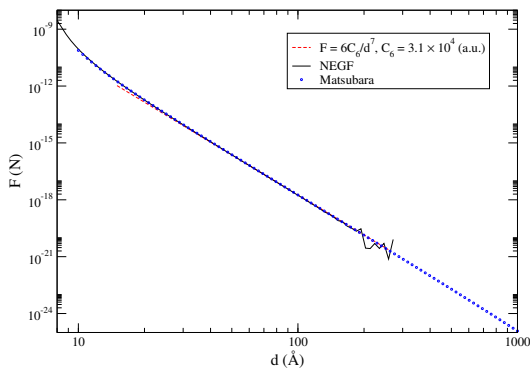


FIG. 4. The force between two C_{60} molecules with center to center distance d at 300 K. The solid line is by the NEGF method; circles are from the Matsubara method. The dashed line is the asymptotic force of $6C_6/d^7$ with a fitted value of the coefficient C_6 for a van der Waals potential.

culations in this paper. The corresponding self-energy $\Pi_{\text{tot}}^r(\omega) = \sum_{j,k,\mu} \Pi_{j\mu,k\mu}^r(\omega)$ is the sum total, i.e., summed over the sites and traced over the direction. We expect $\Pi^r(\omega) \sim \omega^2$ for small frequency, and $3Ne^2/m$ at $\omega \rightarrow \infty$. Here e is the elementary charge unit, m is the effective mass of an electron, and N is the number of electrons. The retarded susceptibility $\chi^r = \sum \Pi^r(1 - v\Pi^r)^{-1}$ is related to the molecule's dynamic polarizability, $\bar{\alpha}(\omega) = -\frac{1}{3}\chi^r(\omega)/\omega^2$. The induced dipole moment is related to the applied electric field by $\mathbf{p} = \bar{\alpha}(\omega)\mathbf{E}$, which defines $\bar{\alpha}(\omega)$. The static polarizability of a C_{60} molecule computed by fitting the ω^2 dependence of χ^r for small ω gives $\bar{\alpha}(0) \approx 460$ a.u. The value is consistent with first principles and experimental results [64–66].

As a check, we consider two identical C_{60} molecules with a center-to-center distance d in thermal equilibrium. Ten baths are weakly coupled to the C_{60} molecules with two of the opposite side pentagons, each connected to independent one-dimensional chains with a coupling strength $\Gamma = -2\text{Im}\Sigma^r = 0.4$ eV to serve as baths. The result of the total van der Waals force between the two C_{60} molecules is plotted in Fig. 4. The result is calculated at 300 K. We compared with the result from the sum of the Matsubara frequency method valid for over-all equilibrium systems. It is seen that the Matsubara method is more accurate for large distances. We also checked the temperature dependence. As expected, the force is insensitive to temperature. From 30 K to 1000 K, the force changes by only about 3%.

The value of the van der Waals coefficient C_6 is found to be 31.3 khartree (bohr)⁶ (i.e., a.u.). This result is about 1/3 of the first principle calculations [66, 67]. The smallness is due to our model. In our tight-binding model, we have one electron per carbon for the π orbitals, and the σ orbitals are absent. Therefore, the transitions of these orbitals to delocalized higher energy states are missing in our treatment. Thus, our force calculations are only qualitative. It appears that the full dynamic polarizability is important to determine the van der Waals

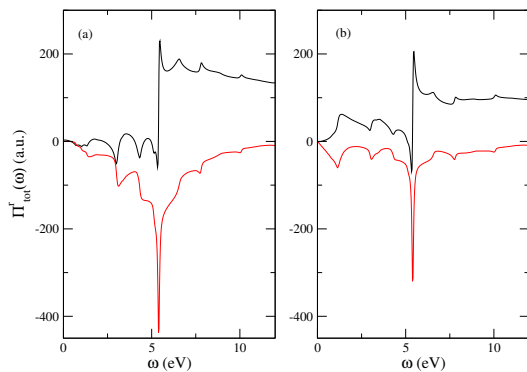


FIG. 5. Sum total of the retarded photon self-energy $\Pi^r(\omega)$ in atomic units for the 13×8 armchair strip with baths. The black line is for the real part, and the red line is for the imaginary part. (a) At chemical potential $\mu = 0$ eV, (b) $\mu = 4$ eV.

force quantitatively. We have also considered other orbitals still within the tight-binding models, the σ orbitals as well as unoccupied d -orbitals [68]. These are important but very expensive to calculate, in order to bring our result to be in agreement with density functional theory-based calculations. Thus, the π -orbital-only model does have a fundamental limitation as far as van der Waals force is concerned.

V. ENERGY AND MOMENTUM TRANSFER BETWEEN C_{60} AND GRAPHENE STRIP

The graphene nanoribbon is modeled with a nearest neighbor hopping model with the same hopping parameter $t = 2.7$ eV as for C_{60} on a part of a honeycomb lattice, with a bond length $a = 1.4$ Å. Conceptually, we use an infinitely long strip with an armchair edge. We cut a section of it (see Fig. 1) as exposed and have electromagnetic interactions, while the remaining two semi-infinite segments serve as baths. The reason for using armchair edges instead of zigzag edges, due to the existence of localized edge states in zigzag configuration, is numerical stability. The qualitative features are the same as zigzag edges.

Figure 5 is an analogous plot as Fig. 3 for the 13×8 nanostrip. Compared to the C_{60} self-energy Π^r , it is smooth instead of several sharp peaks. This is because the spectrum of the electron of an infinitely long strip (due to the two semi-infinite baths) has a continuum. The high peaks are caused by transitions between the energy $-t$ and $+t$ states. At low frequencies at $\mu = 0$ eV (undoped graphene) the values of Π^r are small, while at high chemical potential, it is in a metallic regime, and the value is relatively high.

When each object is in local equilibrium, i.e., the fluctuation-dissipation theorems are valid, the NEGF formulation is equivalent to fluctuational electrodynamics. This means that, in our model, each object is connected to baths that are at the same temperatures and chem-

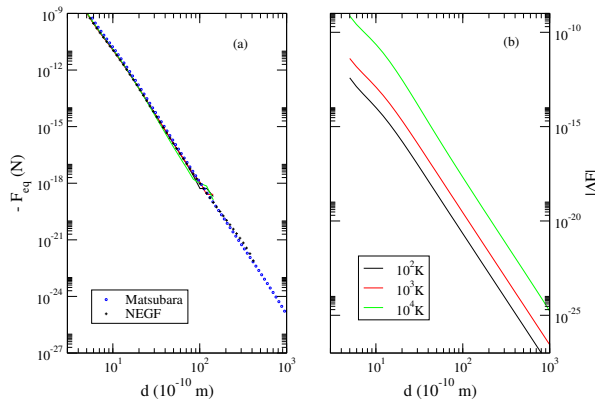


FIG. 6. Force acting on C_{60} by graphene. (a) Force contribution from the first equilibrium term of Eq. (15). Pluses by NEGF and circles from Matsubara method at 300 K. The overlap curves follow the color scheme in (b) for the temperatures of the strip. (b) The nonequilibrium contribution from the second term. The line color indicates strip temperatures.

ical potentials. Then we have $\Pi_\alpha^K = (2N_\alpha + 1)(\Pi_\alpha^r - \Pi_\alpha^a)$. Together with reciprocity, $H^T = H$, which implies $(G^{r,a,<,>})^T = G^{r,a,<,>}$, and $(D^<)^T = D^<$, and $D^a = (D^r)^*$, we can write the force as a sum of an overall equilibrium contribution and a correction due to the nonequilibrium temperature effect, as

$$\mathbf{F}_\alpha = \int_0^\infty \frac{d\omega}{\pi} \text{Tr} \left[\hbar \text{Im}(\nabla D^r \Pi_\alpha^r) (2N_\alpha + 1) \right] + \int_0^\infty \frac{d\omega}{\pi} \text{Tr} \left[\hbar \text{Im} \left(\sum_{\beta \neq \alpha} \delta N_\beta \nabla D^r (\Pi_\beta^r - \Pi_\beta^a) D^a \Pi_\alpha^a \right) \right], \quad (15)$$

where $\delta N_\beta = N_\beta - N_\alpha$. At short distances, it is dominated by the first term as δN_β is small comparing to $2N_\alpha + 1$.

In Fig. 6, we plot the separate contributions from the first term and second term in the force formula above. The temperature of C_{60} is set at 300 K, while the strip is at 100 K (black), 1000 K (red), and 10^4 K (green). The left figure (a) is the equilibrium term. Although we call it equilibrium, strictly speaking, this is not so as the temperatures of the strips are different from that of C_{60} , but the results are insensitive to temperature due to the 1 in $2N_\alpha + 1$. The self-energies of the two objects are only weakly dependent on the temperatures. There is no correction term if the strip is also at 300 K. The correction terms are generally quite small unless the temperature is comparable to the eV energy scale. The sign of the correction is practically determined by δN_β ; it has the same sign as that of the first term if the strip is at a higher temperature than C_{60} , and opposite to that of the first term when the strip is at a lower temperature. Both terms decay with distance as d^{-7} . We could not see the effect of “optical pressure” at these distances.

In a nonequilibrium setting where the local fluctuation-dissipation theorem breaks down, even when the Hamil-

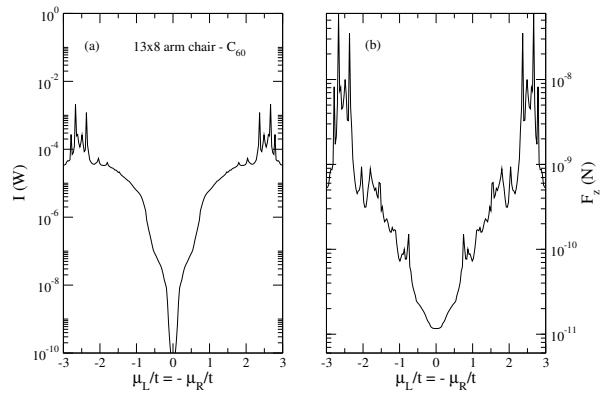


FIG. 7. Transport between 13×8 graphene strip of armchair edge with C_{60} molecule with a center distance $d = 1$ nm away from the graphene at 300 K. The strip is symmetrically biased ($\mu_L = -\mu_R$). (a) Energy transferred to C_{60} , and (b) force in z direction to graphene.

tonian is reciprocal, $H^T = H$, the Green’s functions $G^{>,<}$ and self energies Π^r are no longer reciprocal. This makes a numerical evaluation of the transport quantities rather unstable. There is a large cancellation effect between the first term $D^r \Pi_\alpha^K$ and the second term $D^K \Pi_\alpha^a$ in Eq. (13); they are not simply related to cancel some of the terms, i.e., a Caroli form of the type $\Pi_\beta \cdots \Pi_\alpha$ does not exist. We make sure, numerically to high precision, the known identities are satisfied, such as $G^r - G^a = G^> - G^<$, $\Pi^r - \Pi^a = \Pi^> - \Pi^<$, and the optical theorem $D^r - D^a = D^r (\Pi^r - \Pi^a) D^a$.

The results presented above in Fig. 6 are for the cases where chemical potentials are kept at a constant $\mu = 0$ eV for all the baths. In Fig. 7, we show the situation when the graphene experiences a symmetric bias ($\mu_L = -\mu_R$) of the chemical potentials from the two ends of the graphene strip. The energy transferred to C_{60} and the force applied to the strip are plotted against the chemical potential of the left bath μ_L normalized by the hopping parameter t ; the right bath is set to have the equal and opposite value. Although the temperatures of the two objects are at the same 300 K, the chemical potential bias causes the transfer of energy, which is a nonequilibrium effect. The current flow generates radiation which is transferred to the molecule. The molecule itself is in local thermal equilibrium. The force is of the van der Waals repulsive type. Newton’s third law of the force is valid at our level of approximation. The force applied to C_{60} is exactly equal and opposite to that of graphene plotted to high precision. The value is the smallest (in fact, 0 for the energy transfer) when there is no bias, and it is symmetric about the bias and increases with high biases. At huge biases, we see sharp peaks. These are caused by some resonance of the adsorption/emission. Granted, these values of bias are unrealistic as the system will melt before that. The force in y direction in the graphene plane, perpendicular to the current, is very small (10^{-15} N) due to the structural symmetry. The

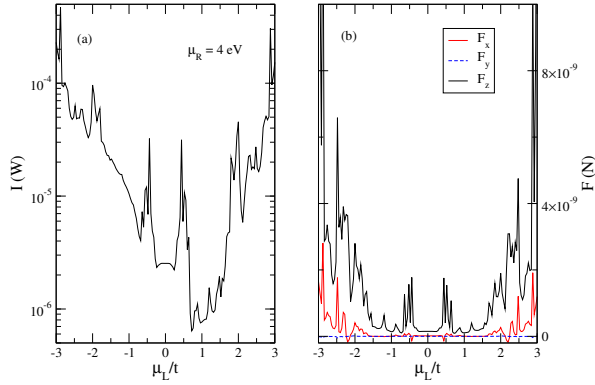


FIG. 8. Transport between 13×8 graphene strip of armchair edge with C_{60} molecule with a center distance $d = 1$ nm away from the graphene at 300 K. The chemical potential of the right side is fixed at $\mu_R = 4$ eV, while scanning the left chemical potential μ_L . (a) Energy transferred to C_{60} , and (b) force in x (red), y (dash), and z (solid black) directions to graphene.

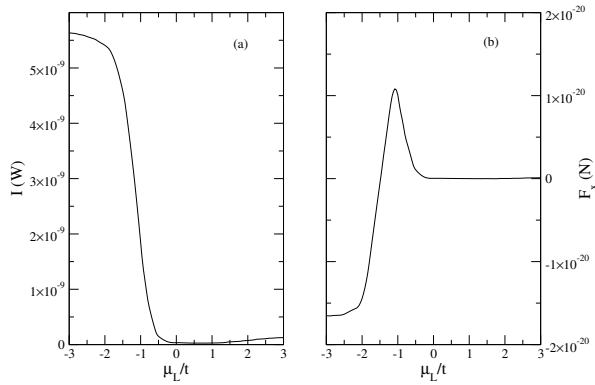


FIG. 9. Transport of combined 13×8 graphene strip and C_{60} molecule to infinity at 300 K. The chemical potential of the right side is fixed at $\mu_R = 4$ eV, while scanning the left chemical potential μ_L . (a) Energy transferred to infinity, and (b) force in x direction acted on the objects.

force in x direction, the direction of the driven current, is also small (peaked at about 10^{-13} N), but it is an odd function of μ_L , reflecting the directionality of the current.

Figure 8 is similar to Fig. 7 except now we fix the right bath at $\mu_R = 4$ eV and scan the value of μ_L . This is not symmetric about 0 or 4 eV. The general feature is the same, i.e., driven current causes a large energy transfer and forces. The attractive force in z direction is still the largest, but now there is a small force in x direction, the sign of which can change. The force in the y direction is still negligibly small. It is clear from the two parameter scans of the chemical potentials that metallic systems give large contributions for both power and force because we have a lot of electrons that can fluctuate, thus inducing interactions.

The radiation of the conserved quantities from systems such as benzene molecules [43], graphene strips [44], or

twisted bilayer graphene has been investigated [69]. We can calculate the transported quantities to infinity using an approximation $D \approx v$ and a multiple expansion of the distances for the Green's function. The resulting formulas are [43–45],

$$-I_\infty = \int_0^\infty d\omega \frac{-\hbar\omega^2}{6\pi^2\epsilon_0 c^3} \text{Im} \sum_{l,l',\mu} \Pi_{l\mu,l'\mu}^<(\omega), \quad (16)$$

$$F_\infty^\mu = \int_0^\infty d\omega \frac{\hbar\omega^3}{60\pi^2\epsilon_0 c^5} \sum_{\alpha,l,l'} \left[4\Pi_{l\alpha,l'\alpha}^<(R_l^\mu - R_{l'}^\mu) - (R_l^\alpha - R_{l'}^\alpha)\Pi_{l\alpha,l'\mu}^< - \Pi_{l\mu,l'\alpha}^<(R_l^\alpha - R_{l'}^\alpha) \right]. \quad (17)$$

As expected, from Fig. 9, we see that the energy and force scales are many orders of magnitudes smaller than the inter-object transfer. Due to the structural symmetry, we do not have angular momentum emission, and the force only has an x component. Large transfers are generated only at a large bias comparable to the hopping parameter $t = 2.7$ eV. Note that the direction of the force changes sign with the bias.

In our formula, Eq. (17), the mutual interaction between C_{60} and graphene is ignored. Under this approximation, each object contributes separately and symmetrically in the z direction, thus, no force in z . In a more precise theory taking the system as a whole and considering the multiple reflections between the objects, it should have a nonzero z component in force due to structural asymmetry.

VI. POWER, FORCE, AND TORQUE BETWEEN TWO IDENTICAL GRAPHENE STRIPS

Finally, in this last section, we present the results of energy, momentum, and angular momentum transfer between two structurally identical strips, except that the top layer is rotated with respect to the bottom one by an angle θ . The two layers are distanced with $d = 1$ nm. In Fig. 10, we plot the quantities against the rotation angle. For the energy transfer, when both strips are in local thermal equilibrium at the same temperature of 300 K, there is no heat transfer (numerically, we get values of the order 10^{-24} W, an indication of the numerical accuracy of our method). When both layers are biased, the values are still very small, of the order 10^{-13} W. The transfer is the largest of the order 10^{-7} W for the case where one of them is at local equilibrium, and the other is biased, as shown in Fig. 10(a).

In Fig. 10(b) the fluctuational force is plotted. The forces are the largest when the system is on top of each other at angles 0 or 90° . It is the smallest when it is 45° . The torque is 0 when it is a multiple of 45° , and oscillating with a period of 90° . Curiously, whether the currents are parallel or anti-parallel, the sign of the force

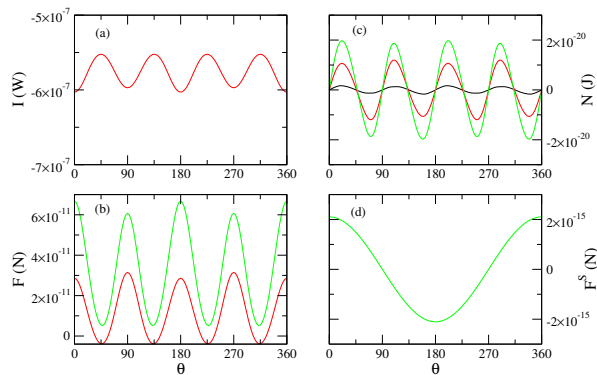


FIG. 10. Transfer of the conserved quantities between two structurally identical 13×8 graphene nanoribbons at 300 K, plotted against the rotation angle from 0 to 360 degrees. For all the subplots, black: $\mu_L = \mu_R = 0$ unbiased for both layers; red: unbiased for the bottom layer, symmetrically biased to the top layer $\mu_L = -\mu_R = -1$ eV; green: both layers are biased by $\mu_L = -\mu_R = -1$ eV. The quantities all refer to the bottom layer. (a) Energy transferred out of the bottom layer. (b) Fluctuational force. (c) Fluctuational torque. (d) Static force based on the Biot-Savart law when both layers are symmetrically biased.

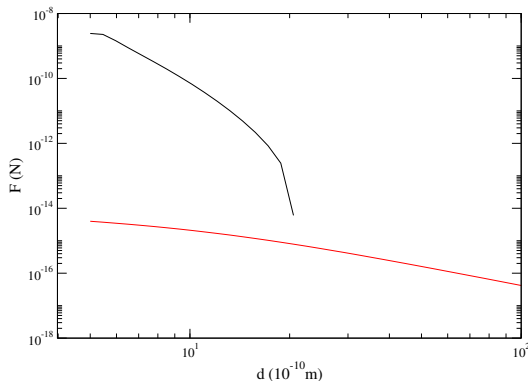


FIG. 11. The fluctuational force (black line) vs. static force (red line) based on the Biot-Savart law, as a function of the distance d . The system is two identical 13×8 graphene strips both at a symmetric bias with parallel currents. The chemical potentials are $\mu_L = -\mu_R = -1$ eV, generating a current of 1.2×10^{-4} A. The temperature is at 300 K.

does not change and remains attractive. We realized that there is another contribution to the force, which is the explicit effect of the current by the Biot-Savart law. This additional correction term is calculated; see Fig. 10(d). At a distance of 1 nm, the static force, in fact, is 4 orders of magnitude smaller, mainly because of the $1/c^2$ factor in the formula, see Eq. (A9).

The force between two rotated strips can become repulsive for certain angles. This anomaly appears generically also for other small structures, such as between two 2×4 armchair ribbons without the leads. We will discuss this issue in the summary section.

At a distance $d = 1$ nm between the graphene ribbons,

the fluctuational force dominates, but it decays much faster as d^{-7} , while the static force decays as d^{-2} . We can give a rough estimate of the cross-over distance. We approximate the van der Waals force by $F_f = E_0 V^2 / d^7$, where E_0 is an energy scale of order eV, while $V = aL^2$ is roughly the volume of the graphene (as the polarizability α is proportional to the volume of the system). The electric current is about $I = \sigma \Delta\mu / e$. We use the conductance $\sigma = e^2 / h$, h is the Planck constant. So the force by Biot-Savart law is about $F_b = (IL)^2 / (d^2 c^2 \epsilon_0)$. The cross-over distance is obtained by equating the two forces, as

$$d \sim \left(\frac{E_0 V^2 4\pi\epsilon_0 c^2 \hbar^2}{e^2 L^2 \Delta\mu^2} \right)^{1/5}. \quad (18)$$

Using the values $E_0 \sim 1$ eV, $L \sim 1.5$ nm, $V \sim 300 \text{ \AA}^3$, $\Delta\mu \sim 2$ eV, we find $d \sim 3$ nm. This is comparable to the actual cross-over distance; see Fig. 11.

VII. SUMMARY

We have given a few applications of the general theory of photon transport between carbon systems. They are the van der Waals force between identical C_{60} molecules, or between C_{60} and graphene flake, or between current-carrying graphene strips. Some more technical details are given, such as the diamagnetic self-energy term. We also relate the NEGF formalism with the fluctuational electrodynamics results when the systems are in thermal equilibrium. The main strength of our formalism is the application in nonequilibrium steady states. In this work, we focus on the chemical potential drive, but a nonequilibrium setting with two baths at different temperatures is straightforward. Our numerical calculations indicate that a current drive generally enhances the transfer of energy and momentum. In addition to the attractive force, the drive can produce extra force in the driven direction. When both objects have direct currents, the additional static Lorentz force is calculated. However, it turns out that this force is about four orders of magnitude smaller at the nanometer scale.

Our systems are relatively small. In order to model larger systems, we need to use shortcuts to reduce the computational complexity. For example, we can approximate the self-energy Π as local, or model Π by a Drude model. Another possibility is to use periodicity to go into wavevector space when one or both systems are infinitely large. The method can be applied to many situations, e.g., systems that are magnetic or in a magnetic field. We can also see drag effects due to current if the electron Green's functions are the interacting ones with an additional electron-photon self-energy of GW type. A periodically driving Floquet system is genuinely a nonequilibrium situation for which our formalism is applied with minor revision [70].

Our numerical approach to the transport problems based on nonequilibrium Green's functions does pose certain difficulties. First, the Meir-Wingreen formula, Eq. (13), contains two terms, which are competing and canceling. It is an intrinsic effect due to the nonequilibrium setting. For local equilibrium systems, alternative equivalent forms, such as the Matsubara frequency version, offer much better numerical stability. Thus, it is instructive to consider perturbative results analytically, focusing on small deviations from the equilibrium result for certain problems, such as small chemical potential bias. Second, there is the divergence at zero distance in the photon Green's functions. In many situations, this divergent term can be dropped; for example, the self-force of an object to itself in equilibrium is zero, but it is not clear we can do such manipulation for nonequilibrium systems. Our approach is to give a cut-off to the distance so that zero distance is forbidden. This regularizes the divergence. In fact, this cut-off has a physical meaning, it is related to the screening of the electrons [57] and to the electric field inside a body [56]. Finally, our random phase approximation combined with the lowest order diamagnetic term may not give correct local gauge invariance. This breakdown of gauge invariance may be the reason we have seen that for certain configurations, we get repulsive forces, which is not correct. To overcome this difficulty, we may have to use other gauges such as the multi-polar gauge through the Power-Zienau-Woolley transform [71, 72]. Even though we have numerical difficulties for some systems, we believe NEGF is still the only offer to treat nonequilibrium systems correctly from a fundamental point of view beyond fluctuational electrodynamics.

ACKNOWLEDGEMENTS

We thank Svend-Age Biehs for an enlightening discussion regarding the static force. J.-S. W is supported by an MOE tier 1 grant A-8000990-00-00. He thanks the group "Theory of Light-Matter and Quantum Phenomena" of the Laboratoire Charles Coulomb for hospitality during his stay in Montpellier, where parts of this work were done. J.-S. W. and M. A. acknowledge CNRS for financial support. M. A. acknowledges support from the French Agence Nationale pour la Recherche – ANR ("CAT" project).

Appendix A: Derivation of the Meir-Wingreen formula

We give a quick and alternative derivation of the Meir-Wingreen formula. By eliminating the charge due to the continuity equation and integrating by parts under the integral sign, we have the energy current, force, and torque, as

$$I = \text{Tr}\langle \dot{\mathbf{A}}\mathbf{j} \rangle, \quad (\text{A1})$$

$$\mathbf{F} = \text{Tr}\langle \nabla\mathbf{A}\mathbf{j} \rangle, \quad (\text{A2})$$

$$\mathbf{N} = \text{Tr}\langle (\mathbf{r} \times \nabla + \epsilon)\mathbf{A}\mathbf{j} \rangle, \quad (\text{A3})$$

here, the notation Tr means integration over the volume of a focusing object (out of several well-separated objects) and trace of the directions; $\mathbf{A}\mathbf{j}$ is interpreted as a dyadic formed by the vector potential \mathbf{A} and current \mathbf{j} , ϵ is a vector tensor, its i -th component is the Levi-Civita symbol $\epsilon_{i\mu\nu}$. The angular brackets denote a steady-state average. We can write the three formulas as a single formula $\text{Tr}\langle \hat{O}/(-i\hbar)\mathbf{A}\mathbf{j} \rangle$ with an appropriate definition of the operator \hat{O} . The energy current is due to the Joule heating, the force and torque are consequences of the Lorentz force.

We can relate the current density to the vector field as $\mathbf{j} = -v^{-1}\mathbf{A} = -\mathbf{A}v^{-1}$. Here $v^{-1} = -\epsilon_0(\partial^2/\partial t^2 + c^2\nabla \times \nabla \times \cdot)$ is a differential operator. Since v is symmetric, acting from the left or right to \mathbf{A} is the same. Using the acting-from-right form, we find $\text{Tr}\langle \hat{O}\mathbf{A}\mathbf{j} \rangle = -\text{Tr}\langle \hat{O}\langle \mathbf{A}\mathbf{A} \rangle v^{-1} \rangle$. The thermal average $\langle \mathbf{A}\mathbf{A} \rangle$ is a shorthand notation for $\langle A_\mu(\mathbf{r}, t)A_\nu(\mathbf{r}', t) \rangle$. The field correlation will be then interpreted as the symmetric version, and can be expressed by $\langle \mathbf{A}\mathbf{A} \rangle = i\hbar D^K(0)/2$. Here, the two \mathbf{A} 's are at different space locations \mathbf{r} or orientations μ but at the same time, so the Green's function in the time domain is at $t = 0$. By working in the Fourier space, we obtain $D^K(0)$ by integrating over frequencies. It is sufficient to integrate over the positive frequencies and multiply by 2 due to symmetry in D^K . So we can write the transported quantities as

$$\frac{d\langle \hat{O} \rangle}{dt} = \text{Re} \int_0^\infty \frac{d\omega}{2\pi} \text{Tr} \left(\hat{O} D^K v^{-1} \right). \quad (\text{A4})$$

We eliminate the operator v^{-1} in favor of Green's functions of D and Π , by the Dyson equation. $D^r = v + v\Pi^r D^r$ implies $v^{-1}D^r = I + \Pi^r D^r$. Here I is the identity operator in (\mathbf{r}, μ) , ω space. Taking the Hermitian conjugate, we get $D^a v^{-1} = I + D^a \Pi^a$. Using the Keldysh equation $D^K = D^r \Pi^K D^a$, and acting by v^{-1} from the right, we find

$$\frac{d\langle \hat{O} \rangle}{dt} = \text{Re} \int_0^\infty \frac{d\omega}{2\pi} \text{Tr} \left[\hat{O} (D^r \Pi^K + D^K \Pi^a) \right]. \quad (\text{A5})$$

Although the self-energy Π here is for all objects, we note that the integration is over only the focused object α ; as a result, we can replace Π by Π_α in the above formula. This is the Meir-Wingreen formula [44, 45, 73].

The above derivation is valid when $\langle \mathbf{A} \rangle = 0$. When it is not zero, the Green's function D appearing in the Dyson equation is the centered one or connected one. We must also take into account a time-independent static piece,

$$\langle \mathbf{A}\mathbf{A} \rangle = i\hbar D + \langle \mathbf{A} \rangle \langle \mathbf{A} \rangle. \quad (\text{A6})$$

This static term does not affect the energy transfer as \hat{O} is a time derivative to the first \mathbf{A} . But it does have

a contribution to the force and torque, an explicit static Lorentz force effect.

To evaluate this static term, we go back to the current; the extra contribution is $-\frac{1}{i\hbar}\text{Tr}(\hat{O}\langle\mathbf{A}\rangle\langle\mathbf{j}\rangle)$. In our discrete representation, the current at site l integrated over a cell volume is $-c^\dagger\mathbf{M}^l c$, where \mathbf{M} has been defined by Eq. (4) in the main texts by the velocity matrix. We use $\mathbf{A} = -v\mathbf{j}$. To the lowest order in the electron-photon interaction, we calculate the discrete current as a column vector \bar{I} with component (l, μ) ,

$$\bar{I}^{l,\mu} = -2 \sum_{j,k} \langle c_j^\dagger M_{jk}^{l\mu} c_k \rangle = 2i\hbar \text{Tr}(G^<(0)M^{l\mu}). \quad (\text{A7})$$

Then we can compute the extra static term to be

$$\frac{1}{i\hbar} \text{Tr} \left[\hat{O} v(\omega=0) \bar{I} (\bar{I}^\alpha)^T \right]. \quad (\text{A8})$$

Here \bar{I} is the current of all objects, while \bar{I}^α is the contribution from the focused object α . Note that if the object α does not carry current, the correction term is 0. The meaning of trace is changed to sum over site index and direction, as we are using a discrete current located on each site.

Apparently, Eq. (A8) is divergent due to $1/\omega$ and $1/\omega^2$ terms in $v(\omega)$, see Eq. (11) in the main texts. The origin of this divergence stems from the fact that the continuity equation does not determine the static charge at $\omega \rightarrow 0$. As a result, the relation $\langle \rho \mathbf{A} \rangle = -\langle \dot{\rho} \mathbf{A} \rangle$ breaks down in the static limit. How much static charge we have has to be a separate model assumption. Since the system must be neutral with the explicit charge of the electrons and the ionic background, we demand that $\langle \rho \rangle = 0$. As a result, the electric field term $\rho \mathbf{E}$ cannot cancel the $-(\mathbf{j} \cdot \nabla) \mathbf{A}$ term leading to Eq. (A2). When this extra term is added, the divergent terms cancel, and we obtain the Biot-Savart law of a pure magnetic field force,

$$\mathbf{F}_\alpha^S = \frac{\mu_0}{4\pi} \sum_{l,l'} \frac{\bar{\mathbf{I}}_l^\alpha \times (\bar{\mathbf{I}}_{l'}^\alpha \times \hat{\mathbf{R}})}{R^2}, \quad (\text{A9})$$

here $\hat{\mathbf{R}} = (\mathbf{R}_l - \mathbf{R}_{l'})/R$ is the unit vector from the source (primed quantities) to the observation point. The torque is similarly calculated by \mathbf{R}_l cross-product with each term in the sum.

Appendix B: From Meir-Wingreen formula to Casimir-Polder formula

In this appendix, we present a derivation of the well-known Casimir-Polder formula for the van der Waals coefficient C_6 from the Meir-Wingreen formula. Let us consider two objects, calling them 1 and 2. The force on object 1 is

$$\mathbf{F}_1 = \text{Re} \int_0^\infty \frac{d\omega}{2\pi} \text{Tr} \left[\frac{\hbar}{i} \nabla (D^r \Pi_1^K + D^K \Pi_1^a) \right]. \quad (\text{B1})$$

Here the trace means summing over the sites and directions. To derive the Casimir-Polder formula, we make some simplifications. The first step is to solve the retarded Dyson equation in block matrix form:

$$\begin{pmatrix} D_{11} & D_{12} \\ D_{21} & D_{22} \end{pmatrix} = \begin{pmatrix} v_{11} & v_{12} \\ v_{21} & v_{22} \end{pmatrix} + \begin{pmatrix} v_{11} & v_{12} \\ v_{21} & v_{22} \end{pmatrix} \begin{pmatrix} \Pi_1 & 0 \\ 0 & \Pi_2 \end{pmatrix} \begin{pmatrix} D_{11} & D_{12} \\ D_{21} & D_{22} \end{pmatrix}. \quad (\text{B2})$$

Here, the matrix Π representing the material properties is block-diagonal. The solution can be explicitly found to be

$$D_{11} = \epsilon_1^{-1} (1 - v_{12} \chi_2 v_{21} \chi_1)^{-1} (v_{11} + v_{12} \chi_2 v_{21}), \quad (\text{B3})$$

$$D_{12} = \epsilon_1^{-1} (1 - v_{12} \chi_2 v_{21} \chi_1)^{-1} v_{12} (\epsilon_2^T)^{-1}, \quad (\text{B4})$$

where we define the dielectric matrix $\epsilon_1 = 1 - v_{11} \Pi_1$, and the susceptibility $\chi_\alpha = \Pi_\alpha \epsilon_\alpha^{-1}$, $\alpha = 1, 2$. The superscript T is the matrix transpose (in site and direction space). We assume that the distance between the two objects is large, so v_{12} and v_{21} are small, but v_{11} and v_{22} are not small. They produce a screening effect. In the limit of long distance, small χ_α , but $v_{\alpha\alpha} \Pi_\alpha$ finite, it is sufficient to keep

$$D_{11} = \epsilon_1^{-1} v_{11} + \epsilon_1^{-1} v_{12} \chi_2 v_{21} (\epsilon_1^T)^{-1} + \dots, \quad (\text{B5})$$

$$D_{21} = \epsilon_2^{-1} v_{21} (\epsilon_1^T)^{-1} + \dots. \quad (\text{B6})$$

The derivative of the Green's function is obtained by taking the derivative of the Dyson equation, $'D = 'v + 'v \Pi D$, where the prime means partial derivative with respect to space of the first argument. To the same order of accuracy, we have, for the derivatives of the photon Green's function,

$$\begin{aligned} 'D_{11} &= \left['v_{11} (1 + \chi_1 v_{12} \chi_2 v_{21}) + 'v_{12} \chi_2 v_{21} \right] (\epsilon_1^T)^{-1} + \dots, \\ 'D_{12} &= ('v_{12} + 'v_{11} \chi_1 v_{12}) (\epsilon_2^T)^{-1} + \dots. \end{aligned} \quad (\text{B7})$$

Putting these expressions into the force formula, we find two types of expressions, these involving only object 1; such terms must be zero as a single object has no force on itself. The terms which are a product of objects 1 and 2 in the self-energies are contributions to the mutual interaction force. We take the zero-temperature limit. Then $\Pi_\alpha^K = \Pi_\alpha^< + \Pi_\alpha^> = \Pi_\alpha^r - \Pi_\alpha^a = 2i \text{Im} \Pi_\alpha^r$. Here, we assume reciprocity in the sense $(\Pi^r)^T = \Pi^r$. We can express the force then as

$$\mathbf{F}_1 = \text{Im} \int_0^\infty \frac{d\omega}{\pi} \text{Tr} \left[\hbar (\nabla v_{12}) \chi_2^r v_{21} \chi_1^r \right]. \quad (\text{B8})$$

In deriving the above, we have used the identity $\chi(\epsilon^{-1})^* - (\epsilon^T)^{-1} \chi^* = \chi - \chi^*$. The two extra terms $'v_{11} \chi_1 + 'v_{11} \chi_1 v_{12} \chi_2 v_{21} \chi_1$ are zero due to symmetry. Such terms take the form $'v_{11} F$, here $F^T = F$, $v_{11}^T = v_{11}$, $v_{11}(\mathbf{r}, \mathbf{r}') = v_{11}(\mathbf{r}', \mathbf{r})$, and $'v_{11} = -v_{11}'$. Here $'v$ denotes derivative to

the first argument, and v' is derivative to the second argument. Using integration by parts (due to the trace sign), we can move the space derivative around in two ways. We find $v_{11}F' = -v_{11}'F$, so it must be zero exactly. For near distances, if we take into account multiple reflections, the formula (B8) needs to be revised by a replacement $v_{21} \mapsto (1 - v_{21}\chi_1v_{12}\chi_2)^{-1}v_{21}$ [47].

We take the non-retardation limit (that is, $c \rightarrow \infty$). The free field Green's function simplifies to

$$v = v^r = v^a \approx \frac{1}{4\pi\epsilon_0\omega^2r^3}(\overleftrightarrow{\mathbf{U}} - 3\hat{\mathbf{R}}\hat{\mathbf{R}}). \quad (\text{B9})$$

In this limit, v is real, representing the dipole interaction. We assume the distance r between the two objects is much larger than the sizes of the molecules, so in evaluating v , we can take the second molecule all at the origin and the first molecule all at $(0, 0, r)$. As a result, v_{jk} no longer depends on the site indices. The summation over the sites is carried out only for the self-energies. We also assume that the site summed χ_α^r is isotropic and is proportional to the identity. We are able to relate the “total” $\Pi^r\epsilon^{-1}$ to the isotropic polarizability $\bar{\alpha}$. The site summed χ^r is the linear response to the volume integrated current density, $\int j_\mu dV = -\sum_{l,\nu} \chi_{l\mu,\nu}^r A_\nu^{\text{ext}}$. We can write the current as charge density times velocity, which in turn can be written as the rate of change of dipole moment; thus, $(-i\omega)\mathbf{p} = -\frac{1}{3}\chi^r(\omega)_{\text{tot}}\mathbf{A}$. Here, we define a scalar quantity

$$\chi_{\text{tot}}^r(\omega) = \sum_{l,\nu,\mu} \chi_{l\mu,\nu}^r(\omega) = -3\omega^2\bar{\alpha}(\omega). \quad (\text{B10})$$

The ω^2 factor is due to $\frac{d}{dt}\mathbf{p} = \int \mathbf{j} dV$, $\mathbf{E} = -d\mathbf{A}/dt$, and in the frequency domain, the time derivative is $-i\omega$. Replacing χ^r by the isotropic $\bar{\alpha}$, multiplying the matrices in the x, y, z direction space, and taking the trace (which gives a factor of 6), we obtain,

$$F_1^z = \frac{3\hbar}{\pi} \int_0^\infty d\omega \left(\frac{1}{4\pi\epsilon_0} \right)^2 \text{Im} [\bar{\alpha}_1(\omega)\bar{\alpha}_2(\omega)] \left(\frac{-6}{r^7} \right). \quad (\text{B11})$$

We can now identify the coefficient C_6 as the factor in front of $(-6/r^7)$. The final step is to make a Wick's rotation by integrating over the positive imaginary axis from 0 to $i\infty$. Since the retarded response function or product of retarded Green's functions are still retarded, the integrand is analytic on the upper half-plane. This leads to the final Casimir-Polder expression in the non-retarded limit as [22],

$$C_6 = \frac{3\hbar}{\pi} \left(\frac{1}{4\pi\epsilon_0} \right)^2 \int_0^\infty d\omega' \bar{\alpha}_1(i\omega')\bar{\alpha}_2(i\omega'). \quad (\text{B12})$$

In doing this, taking the imaginary part becomes taking the real part, as $\omega = i\omega'$, but the analytically continued response functions are real on the imaginary axis.

We have used Eq. (B11) of the real frequency formula to compute C_6 for the C_{60} with C_{60} interaction. The numerical value is $\sim 3.07 \times 10^4$ a.u., in good agreement with a direct fit to the distance dependence of the force.

-
- [1] J. R. Howell, M. P. Mengčü, K. Duan, and R. Siegel, *Thermal Radiation Heat Transfer*, 7th ed. (CRC Press, 2020).
- [2] C. M. Hargreaves, Anomalous radiative transfer between closely-spaced bodies, *Phys. Lett.* **30A**, 491 (1969).
- [3] G. A. Domoto, R. F. Boehm, and C. L. Tien, Experimental investigation of radiative transfer between metallic surfaces at cryogenic temperatures, *J. Heat Transf.* **92**, 412 (1970).
- [4] D. Polder and M. van Hove, Theory of radiative heat transfer between closely spaced bodies, *Phys. Rev. B* **4**, 3303 (1971).
- [5] A. Kittel, W. Müller-Hirsch, J. Parisi, S.-A. Biehs, D. Reddig, and M. Holthaus, Near-field heat transfer in a scanning thermal microscope, *Phys. Rev. Lett.* **95**, 224301 (2005).
- [6] S. Shen, A. Narayanaswamy, and G. Chen, Surface phonon polaritons mediated energy transfer between nanoscale gaps, *Nano Lett.* **9**, 2909 (2009).
- [7] R. S. Ottens, V. Quetschke, S. Wise, A. A. Alemi, R. Lundock, G. Mueller, D. H. Reitze, D. B. Tanner, and B. F. Whiting, Near-field radiative heat transfer between macroscopic planar surfaces, *Phys. Rev. Lett.* **107**, 014301 (2011).
- [8] K. Kim, B. Song, V. Fernández-Hurtado, W. Lee, W. Jeong, L. Cui, D. Thompson, J. Feist, M. T. H. Reid, F. J. García-Vidal, J. C. Cuevas, E. Meyhofer, and P. Reddy, Radiative heat transfer in the extreme near field, *Nature* **528**, 387 (2015).
- [9] L. Cui, W. Jeong, V. Fernández-Hurtado, J. Feist, F. J. García-Vidal, J. C. Cuevas, E. Meyhofer, and P. Reddy, Study of radiative heat transfer in ångström- and nanometre-sized gaps, *Nature Comm.* **8**, 14479 (2017).
- [10] K. Kloppstech, N. Können, S.-A. Biehs, A. W. Rodriguez, L. Worbes, D. Hellmann, and A. Kittel, Giant heat transfer in the crossover regime between conduction and radiation, *Nature Comm.* **8**, 14475 (2017).
- [11] A. I. Volokitin and B. N. J. Persson, Near-field radiative heat transfer and noncontact friction, *Rev. Mod. Phys.* **79**, 1291 (2007).
- [12] S. Basu, Z. M. Zhang, and C. J. Fu, Review of near-field thermal radiation and its application to energy conversion, *Int. J. Energy Res.* **33**, 1203 (2009).
- [13] B. Song, A. Fiorino, E. Meyhofer, and P. Reddy, Near-field radiative thermal transport: From theory to experiment, *AIP Advances* **5**, 053503 (2015).
- [14] C. Henkel, Nanoscale thermal transfer – an invitation to fluctuation electrodynamics, *Zeitschrift für Naturforschung A* **72**, 99 (2017).
- [15] S.-A. Biehs, R. Messina, P. S. Venkataram, A. W. Rodriguez, J. C. Cuevas, and P. Ben-Abdallah, Near-field radiative heat transfer in many-body systems, *Rev. Mod. Phys.* **93**, 025009 (2021).
- [16] O. Marconot, A. Juneau-Fecteau, and L. G. Fréchette, Toward applications of near-field radiative heat transfer with micro-hotplates, *Scientific Rep.* **11**, 14347 (2021).
- [17] F. London, The general theory of molecular forces, *Trans. Faraday Soc.* **33**, 8 (1937).
- [18] H. B. G. Casimir, On the attraction between two perfectly conducting plates, *Proc. K. Ned. Akad. Wet* **51**, 793 (1948).
- [19] E. M. Lifshitz, The theory of molecular attractive forces between solids, *Soviet Phys. JETP* **2**, 73 (1956).
- [20] G. L. Klimchitskaya, U. Mohideen, and V. M. Mostepanenko, The Casimir force between real materials: Experiment and theory, *Rev. Mod. Phys.* **81**, 1827 (2009).
- [21] C. Abbas, B. Guizal, and M. Antezza, Strong thermal and electrostatic manipulation of the Casimir force in graphene multilayers, *Phys. Rev. Lett.* **118**, 126101 (2017).
- [22] H. B. G. Casimir and D. Polder, The influence of retardation on the London-van der Waals forces, *Phys. Rev.* **73**, 360 (1948).
- [23] P. W. Milonni, *The Quantum Vacuum: An Introduction to Quantum Electrodynamics* (Academic Press, 1993).
- [24] C. Henkel, K. Joulain, J.-P. Mulet, and J.-J. Greffet, Radiation forces on small particles in thermal near fields, *J. Opt. A: Pure Appl. Opt.* **4**, S109 (2002).
- [25] M. Antezza, L. P. Pitaevskii, and S. Stringari, New asymptotic behavior of the surface-atom force out of thermal equilibrium, *Phys. Rev. Lett.* **95**, 113202 (2005).
- [26] M. Antezza, L. P. Pitaevskii, S. Stringari, and V. B. Svetovoy, Casimir-Lifshitz force out of thermal equilibrium and asymptotic nonadditivity, *Phys. Rev. Lett.* **97**, 223203 (2006).
- [27] M. Antezza, Surface-atom force out of thermal equilibrium and its effect on ultra-cold atoms, *J. Phys. A: Math Gen* **39**, 6117 (2006).
- [28] J. M. Obrecht, R. J. Wild, M. Antezza, L. P. Pitaevskii, S. Stringari, and E. A. Cornell, Measurement of the temperature dependence of the Casimir-Polder force, *Phys. Rev. Lett.* **98**, 063201 (2007).
- [29] R. Messina and M. Antezza, Scattering-matrix approach to Casimir-Lifshitz force and heat transfer out of thermal equilibrium between arbitrary bodies, *Phys. Rev. A* **84**, 042102 (2011).
- [30] Y. Jeyar, K. Austry, M. Luo, B. Guizal, H. B. Chan, and M. Antezza, Casimir-Lifshitz force between graphene-based structures out of thermal equilibrium, *Phys. Rev. B* **108**, 115412 (2023).
- [31] B. van Duppen, A. Tomadin, A. N. Grigorenko, and M. Polini, Current-induced birefringent absorption and non-reciprocal plasmons in graphene, *2D Mater.* **3**, 015011 (2016).
- [32] T. A. Morgado and M. G. Silveirinha, Negative Landau damping in bilayer graphene, *Phys. Rev. Lett.* **119**, 133901 (2017).
- [33] B. Shapiro, Fluctuation-induced forces in the presence of mobile carrier drift, *Phys. Rev. B* **96**, 075407 (2017).
- [34] D. Svintsov and V. Ryzhii, Comment on “negative Landau damping in bilayer graphene”, *Phys. Rev. Lett.* **123**, 219401 (2019).
- [35] R. Messina, W. Jin, and A. W. Rodriguez, Strongly coupled near-field radiative and conductive heat transfer between planar bodies, *Phys. Rev. B* **94**, 121410 (2016).
- [36] M. R. Messina and P. Ben-Abdallah, Conduction-radiation coupling between two closely separated solids, *Phys. Rev. Lett.* **125**, 224302 (2020).
- [37] M. Reina, C. G. Ali Barura, P. Ben-Abdallah, and R. Messina, Conduction-radiation coupling between two distant solids interacting in near-field regime (2023),

- arXiv:2305.10105.
- [38] W. A. Callahan, D. Feng, Z. M. Zhang, E. S. Toberer, A. J. Ferguson, and E. J. Tervo, Coupled charge and radiation transport processes in thermophotovoltaic and thermoradiative cells, *Phys. Rev. Applied* **15**, 054035 (2021).
- [39] L. V. Keldysh, diagram technique for nonequilibrium processes, *Soviet. Phys. JETP* **20**, 1018 (1965).
- [40] H. Haug and A.-P. Jauho, *Quantum Kinetics in Transport and Optics of Semiconductors*, 2nd ed. (Springer-Verlag, 2008).
- [41] J.-S. Wang, J. Wang, and J. T. Lü, Quantum thermal transport in nanostructures, *Eur. Phys. J. B* **62**, 381 (2008).
- [42] J.-S. Wang, B. K. Agarwalla, H. Li, and J. Thingna, Nonequilibrium green's function method for quantum thermal transport, *Front. Phys.* **9**, 673 (2014).
- [43] Z.-Q. Zhang, J.-T. Lü, and J.-S. Wang, Angular momentum radiation from current-carrying molecular junctions, *Phys. Rev. B* **101**, 161406 (2020).
- [44] Y.-M. Zhang, T. Zhu, Z.-Q. Zhang, and J.-S. Wang, Microscopic theory of photon-induced energy, momentum, and angular momentum transport in the nonequilibrium regime, *Phys. Rev. B* **105**, 205421 (2022).
- [45] J.-S. Wang, J. Peng, Z.-Q. Zhang, Y.-M. Zhang, and T. Zhu, Transport in electron-photon systems, *Front. Phys.* **18**, 43602 (2023).
- [46] M. Krüger, T. Emig, and M. Kardar, Nonequilibrium electromagnetic fluctuations: Heat transfer and interactions, *Phys. Rev. Lett.* **106**, 210404 (2011).
- [47] M. Krüger, G. Bimonte, T. Emig, and M. Kardar, Trace formulas for nonequilibrium Casimir interactions, heat radiation, and heat transfer for arbitrary objects, *Phys. Rev. B* **86**, 115423 (2012).
- [48] G. Bimonte, T. Emig, M. Kardar, and M. Krüger, Nonequilibrium fluctuational quantum electrodynamics: heat radiation, heat transfer, and force, *Annu. Rev. Condense. Matter Phys.* **8**, 119 (2017).
- [49] S. Datta, *Electronic Transport in Mesoscopic Systems* (Cambridge Univ. Press, 1995).
- [50] R. Peierls, Zur theorie des diamagnetismus von leitungslektronen, *Z. Physik* **80**, 763 (1933).
- [51] S. M. Rytov, *Theory of Electric Fluctuations and Thermal Radiation* (Air Force Cambridge Research Center, Bedford, MA, 1953).
- [52] S. M. Rytov, Y. A. Kravtsov, and V. I. Tatarskii, *Principles of Statistical Radiophysics 3* (Springer, Berlin, 1989).
- [53] G. D. Mahan, *Many-Particle Physics*, 3rd ed. (Kluwer Academic, 2000).
- [54] L. Novotny and B. Hecht, *Principles of Nano-Optics*, 2nd ed. (Cambridge Univ. Press, 2012).
- [55] O. Keller, *Quantum Theory of Near-Field Electrodynamics* (Springer, Berlin, 2011).
- [56] A. Yaghjian, Electric dyadic Green's functions in the source region, *Proceedings of the IEEE* **68**, 248 (1980).
- [57] S. Thongrattanasiri, A. Manjavacas, and F. J. G. de Abajo, Quantum finite-size effects in graphene plasmons, *ACS Nano* **6**, 1766 (2012).
- [58] B. Strekha, S. Molesky, P. Chao, M. Krüger, and A. W. Rodriguez, Trace expressions and associated limits for nonequilibrium casimir torque, *Phys. Rev. A* **106**, 042222 (2022).
- [59] J. M. Wylie and J. E. Sipe, Quantum electrodynamics near an interface, *Phys. Rev. A* **30**, 1185 (1984).
- [60] G. Bimonte, T. Emig, N. Graham, and M. Kardar, Something can come of nothing: Surface approaches to quantum fluctuations and the Casimir force, *Annu. Rev. Nucl. Part. Sci.* **72**, 93 (2022).
- [61] G. Gómez-Santos, Thermal van der Waals interaction between graphene layers, *Phys. Rev. B* **80**, 245424 (2009).
- [62] P. Senn, Computation of the Cartesian coordinates of Buckminsterfullerene, *J. Chem. Educ.* **72**, 302 (1995).
- [63] S. Satpathy, Electronic structure of the truncated-icosahedral C₆₀ cluster, *Chem. Phys. Lett.* **130**, 545 (1986).
- [64] Y. Wang, G. F. Bertsch, and D. Tománek, Hyperpolarizability of the C₆₀ fullerene cluster, *Z Phys D - Atoms, Molecules and Clusters* **25**, 181 (1993).
- [65] R. R. Zope, T. Baruah, M. R. Pederson, and B. I. Dunlap, Static dielectric response of icosahedral fullerenes from C₆₀ to C₂₁₆₀ characterized by an all-electron density functional theory, *Phys. Rev. B* **77**, 115452 (2008).
- [66] K. U. Lao, Y. Yang, and R. A. DiStasio Jr., Electron confinement meet electron delocalization: non-additivity and finite-size effects in the polarizabilities and dispersion coefficients of the fullerenes, *Phys. Chem. Chem. Phys.* **23**, 5773 (2021).
- [67] J. Kauczor, P. Norman, and W. A. Saidi, Non-additivity of polarizabilities and van der waals c6 coefficients of fullerenes, *J. Chem. Phys.* **138**, 114107 (2013).
- [68] H. Pan, (2024), unpublished. We thank Dr. Hui Pan for this calculation.
- [69] Y.-M. Zhang, M. Antezza, and J.-S. Wang, Controllable thermal radiation from twisted bilayer graphene, *Int. J. Heat Mass Transf* **194**, 123076 (2022).
- [70] G. Tang and J.-S. Wang, Modulating near-field thermal transfer through temporal drivings: a quantum many-body theory, *Phys. Rev. B* **109**, 085428 (2024).
- [71] C. Cohen-Tannoudji, J. Dupont-Roc, and G. Grynberg, *Photons and Atoms: introduction to quantum electrodynamics* (Wiley, 1989).
- [72] M. Schüler, J. A. Makrs, Y. Murakami, C. Jia, and T. P. Devereaux, Gauge invariance of light-matter interactions in first-principle tight-binding models, *Phys. Rev. B* **103**, 155409 (2021).
- [73] Y. Meir and N. S. Wingreen, Landauer formula for the current through an interacting electron region, *Phys. Rev. Lett.* **68**, 2512 (1992).